Clim. Past Discuss., 8, 4989–5027, 2012
www.clim-past-discuss.net/8/4989/2012/
doi:10.5194/cpd-8-4989-2012

Climate of the Past Discussions

Thermomagnetic properties of vivianite nodules, Lake El'gygytgyn, Northeast Russia

P. S. Minyuk[1], T. V. Subbotnikova[1], L. L. Brown[2], and K. J. Murdock[2]

[1]North-East Interdisciplinary Scientific Research Institute of Far East Branch of Russian Academy Science, Magadan, Russia
[2]Department of Geosciences, University of Massachusetts, Amherst, USA

Received: 7 September 2012 – Accepted: 20 September 2012 – Published: 9 October 2012

Correspondence to: P. S. Minyuk (minyuk@neisri.ru)

Published by Copernicus Publications on behalf of the European Geosciences Union.

Abstract

Vivianite, a hydrated iron phosphate, is abundant in sediments of El'gygytgyn Lake, located in the Anadyr Mountains of Central Chukotka, Northeastern Russia (67°30′ N; 172°05′ E). Magnetic measurements, including weight low-field AC magnetic susceptibility, field dependent magnetic susceptibility, hysteresis parameters, temperature dependence of the saturation magnetization, as well as susceptibility in different heating media provide ample information on vivianite. Electron-microprobe analyses, electron microscopy and energy dispersive spectroscopy were used to identify diagnostic minerals. Vivianite nodules are abundant in both sediments of cold (anoxic) and warm (oxic) stages. Magnetic susceptibility of the nodules varies from 0.78×10^{-6} m^3 kg^{-1} to 1.72×10^{-6} m^3 kg^{-1} (average = 1.05×10^{-6} m^3 kg^{-1}) and is higher than the susceptibility of sediments from the cold intervals. Magnetic properties of vivianite are due to product of oxidation as well as sediment and mineral inclusions. Three types of curves of high temperature dependence susceptibility of vivianite indicate different degree of oxidation and inclusions in the nodules. Vivianite acts as a reductant and reduces hematite to magnetite and suppresses the goethite-hematite transition during heating. Heating vivianite and sulfur mixture stimulate the formation of monoclinic pyrrhotite. An additive of arsenic inhibits the formation of magnetite prior to its Curie temperature. Heating selective vivianite and pyrite mixtures produces formation of several different minerals – magnetite, monoclinic pyrrhotite, and hexagonal pyrrhotite, and make it difficult to interpret the thermomagnetic curves.

1 Introduction

Vivianite, $Fe_3(PO_4)_2 \cdot 8H_2O$, is an hydrated iron phosphate that has long been identified in variety of natural environments. This authigenic mineral forms when anoxic environments provide readily available ferric iron, usually dissolution products of iron oxides, and inorganic phosphorous. It has been found as a secondary mineral in wide

CPD
8, 4989–5027, 2012

range of situations including weathering products of hydrothermal deposits, Fe-bearing ore veins, reducing soils and aquifers, and lacustrine and marine reduced sediments. The presence of vivianite in lake sediments is well documented, and it has been the subject of detailed studies in many lacustrine environments from large lakes such as Lake Baikal (Fagel et al., 2005; Sapota et al., 2006), to small mesotropic lakes in the Canadian prairie (Manning et al., 1991, 1999) to Holocene muds in Norway (Rosenquist, 1970) to Lago Maggiore, Italy (Nembrin et al., 1983). The formation of authigenic vivianite in lake sediments is not fully understood, but appears to be influenced by redox conditions, pH values, dissolved elements, primarily Fe and P, but often including impurities of Ca, Mn, and Mg, organic matter content, and sedimentation rate (Sapota et al., 2006). Vivianite is usually a stable mineral in environments over the pH range of 6 to 9 and low Eh values of less than 0.0 (Nriagu and Dell, 1974). Vivianite is found as small disaggerate crystals to large nodules, often several centimeters in diameter. In air vivianite readily oxidizes, turning from opaque or white to vivid blue in a short time, eventually altering to metavivianite (kerchenite) (Rodgers, 1986) or santabarbaraite (Pratesi et al., 2003), as the original Fe^{2+} becomes completely replaced by Fe^{3+}. The magnetic properties of vivianite are well-known (Meijer et al., 1967), and although it is paramagnetic in natural environments and surface temperature, it becomes antiferromagnetic at exceedingly low temperature with a Néel temperature of $\sim 12\,K$ (Meijer et al., 1967; Frederichs et al., 2003). Maximum magnetic susceptibility of vivianite ($6.62 \times 10^{-6}\,m^3\,kg^{-1}$) is observed at the Néel temperature (Frederichs et al., 2003); at room temperature the susceptibility is close to $1 \times 10^{-6}\,m^3\,kg^{-1}$. In this paper we investigate the magnetic properties, especially those at high temperature, for vivianite nodules found in the sediments of Lake El'gygytgyn in Northeast Siberia. Although vivianite is paramagnetic at room temperature, studies of nodules of the material investigate the presence or absence of magnetite grains within the vivianite, and shed light on the magnetic properties of lake sediments where vivianite is common.

CPD
8, 4989–5027, 2012

2 Geologic setting

Vivianite was studied from sediments of El'gygytgyn Lake, located in the Anadyr Mountains of Central Chukotka, Northeastern Russia (67° 30′ N; 172° 05′ E) (Fig. 1). The lake is situated in a 3.6 Ma impact crater located in a series of volcanic rocks (rhyodacite ignimbrites, rhyolite to andesite tuffs, and basalt flows) of late Cretaceous age (Bely and Belaya, 1998; Bely and Raikevich, 1994; Gurov et al., 2007; Layer, 2000). Sediment input to the lake is controlled by a series of some 50 small inlet streams draining the crater; output from the lake is only by one stream, the Enmyvaam River, flowing southeast from the crater to the Bering Sea (Nolan and Brigham-Grette, 2007). Preliminary studies and short cores collected from the lake (Brigham-Grette et al., 2007) attested to the suitability of lake El'gygytgyn sediments to provide a detailed climate record for this High Arctic site. Additional deep drilling was done in 2008–2009, when over 318 m of sediment core and 200 m of impact breccia was extracted by ICDP at site 5011 in the lake (Melles et al., 2011), providing a vast amount of material to be studied for paleoclimate information (Melles et al., 2012, and papers within this issue). Chronology of the entire package has been established using paleomagnetic time scale with detailed tuning to the marine oxygen isotope record and insolation variations (Nowaczyk et al., 2012).

Vivianite has been identified extensively in the earlier, shorter cores (Asikainen et al., 2007; Minyuk et al., 2007) using both observational and laboratory techniques, and interpreted as forming under anoxic conditions when phosphorus and iron were both plentiful. Fine-grained dispersed vivianite has been recognized using low-temperature magnetic measurements (Murdock et al., 2012). Due to the ubiquitous occurrence of vivianite as both small grains and larger rounded aggregates or nodules, Minyuk et al. (2007) conclude its formation is controlled by diagenetic microenvironments and not influenced by large-scale climate conditions.

CPD
8, 4989–5027, 2012

3 Materials and method

Vivianite nodules and pieces were collected down continuous core (Core 1A, 1B of ICDP site 5011) from 5 to 28 m in depth (Melles et al., 2012). Both sediment and nodules were retained for study, with the nodules separated from lake sediment by sieving, using a 250 µm sieve. The nodules were analyzed using a range of thermomagnetic and mineralogical methods at the North-East Interdisciplinary Scientific Research Institute of Far East Branch of Russian Academy of Science. Weight low-field AC magnetic susceptibility, as well as field dependent and frequency dependent magnetic susceptibility were measured on kappabridge MFK1-FA (AGICO Ltd., Brno, Czech Republic). Hysteresis parameters, including the saturation magnetization (J_s), induced magnetization (J_i), saturation remanence (J_{rs}), coercive force (H_c), and remanence coercivity (H_{cr}) were measured by an automatic coercive spectrometer (Burov et al., 1986). The temperature dependence of the saturation magnetization (J_s-T) was measured on a Curie express balance (Burov et al., 1986) in field 500 mT with heating rate of 100 °min^{-1}. Temperature-dependent susceptibility (k-T) of crushed nodules was measured continuously from room temperature up to 700 °C and back to room temperature using a kappabridge MFK1-FA equipped with a CS-3 high-temperature furnace (AGICO Ltd., Brno, Czech Republic). The heating and cooling rates were 10–12 °C min^{-1}.

Electron-microprobe (EMP) analyses of polished nodules mounted in epoxy resin were performed using "Camebax". Acceleration voltage of 25 kV and electron-beam spot-size of 4 µm was used. Specimens for scanning electron microscopy (SEM) and energy dispersive spectroscopy (EDS) analyses were mounted on aluminum studs and carbon-coated. The SEM-EDS analyses have been carried out using QEMSCAN system including scanning electron microscopy (EVO-50) with energy dispersive X-ray spectroscopy Quantax Espirit (Bruker).

The chemical composition and major elements in the lake sediments minus the nodules were analyzed using a multichannel X-ray fluorescence (XRF) spectrometer

CPD
8, 4989–5027, 2012

SRM-25 (USSR) and S4 Pioneer X-ray fluorescence spectrometer (Bruker, Germany). Elemental compositions were determined using the fundamental parameters method (Borkhodoev, 2002).

4 Results

Vivianite nodules range in size up to 3 cm. They are composed of crystal aggregates often having spherical morphology, sometimes crystal clusters or flat crusts. Surface of nodules is darker then inner parts, with a striking bluish to greenish color appearing on the surface with oxidation. Many spherical nodules are empty in the central parts or consist of visible crystals clusters; morphologies of inner and outer parts of typical nodules are illustrated in Fig. 2.

4.1 Microprobe analyses – sediments and nodules

Electron-microprobe quantitative analyses of 10 selected nodules reveal the presence of Fe_2O_3, P_2O_5 and MnO. The average content of Fe_2O_3 is 35.18 %, with a range from 30.18 to 39.4 %. P_2O_5 displays values between 21.23–29.28 % (average 25.02 %) with MnO concentration varying from 0.67 to 6.34 % (average 2.06 %) (Table 1). The ratio of phosphorous to manganese in the vivianite samples range from 4.61 to 37.45.

Major elements determination was performed on sediment samples from which vivianite nodules were removed. Figure 3 shows the distribution of Fe_2O_3, P_2O_5, MnO along the depth profile. Distribution of both P_2O_5 and MnO are synchronous in this section, whereas Fe_2O_3 appears to vary independent of P_2O_5 and MnO, with some intervals showing strong correlations, but other regions where low Fe_2O_3 content corresponds to the phosphorous and manganese highs. For all samples the coefficient correlation between P_2O_5 and MnO is 0.55, between Fe_2O_3 and P_2O_5 is 0.55. Distribution of phosphorous and manganese shows few levels with higher concentrations of these elements – depth intervals 8.71–9.21, 11.51–12.19, 13.19–13.51, 18.39–18.85,

CPD
8, 4989–5027, 2012

20.95–21.17, 24.31–24.73 m (Fig. 3, Table 2). Geochemical data suggest that fine-grained vivianite minerals are present at these levels. Smear slides prepared from sediments in the indicated regions reveal blue, greenish vivianite aggregates and broken pieces of fine concretions. A maximum amount of the oxides in these zones are Fe_2O_3 – 13.54 %, P_2O_5 – 4.02 %, MnO – 0.91 %.

4.2 Scanning electron microscopy and energy dispersive spectroscopy

In most cases, the vivianite concretions studied are not homogeneous, but contain irregular oxidized patches as well as discrete mineral inclusions. Ten polish nodules were studied by electron microscopy (SEM) and energy dispersive spectroscopy (EDS). Backscatter images with accompanying EDS elemental scans are shown in Fig. 4. As can be observed in Fig. 4a, b, the lighter colored parts of the backscattered electron images have higher contents of Fe and P. Some of the studied vivianite nodules were attracted to magnet in hand sample. A few of these "magnetic" nodules were crushed and the resulting magnetic extract was studied using SEM and EDS. In a few grains sulfides of Fe, presumably greigite, were found (Fig. 4c), identified by the presence of iron and sulfur, and the absence of phosphorous. Semiquantitative composition of sulfide is Fe = 46.20–50.23 norm. wt %, S = 35.62–33.26 norm. wt %, Ni = 2.31–2.77 norm. wt %, and a few percent of Mg, Al, K, and Si. In some nodules ilmenite was identified (Fig. 4d) by the combined presence of iron and titanium, with a compositon of Fe = 38.30–42.58, Ti = 29.31–34.86, O = 21.93–28.54, Al and Si < 1 %. Although rare, in a few samples Fe-rich phases were found, with iron (Fe = 82.87–92.90 norm. wt %) the main constituent and only a few % P, Mn, and Si. All the nodules investigated were found to included minor minerals with high content of Si, Al, and Na. On the electron images these minerals look like dark patches and take on several different forms and sizes.

CPD
8, 4989–5027, 2012

4.3 Magnetic susceptibility of vivianite nodules

Nodules were found in sediments with both high and low magnetic susceptibility (Fig. 3, Table 3). In general, magnetic susceptibility of the sediment section studied here varies from $0.09 \times 10^{-6}\,m^3\,kg^{-1}$ to $5.12 \times 10^{-6}\,m^3\,kg^{-1}$ (average $0.95 \times 10^{-6}\,m^3\,kg^{-1}$).

Magnetic susceptibility of nodules ($n = 54$) shows values between $0.78 \times 10^{-6}\,m^3\,kg^{-1}$ and $1.72 \times 10^{-6}\,m^3\,kg^{-1}$ (average = $1.05 \times 10^{-6}\,m^3\,kg^{-1}$). These values are much higher then those from the low MS intervals in core sediments.

MS of bulk sediments from low magnetic intervals ranges from $0.09 \times 10^{-6}\,m^3\,kg^{-1}$ to $1.73 \times 10^{-6}\,m^3\,kg^{-1}$ (average $0.39 \times 10^{-6}\,m^3\,kg^{-1}$), $n = 583$. From the high magnetic intervals, the MS of bulk sediments varies between $0.18 \times 10^{-6}\,m^3\,kg^{-1}$ and $5.12 \times 10^{-6}\,m^3\,kg^{-1}$ (average $1.8 \times 10^{-6}\,m^3\,kg^{-1}$), $n = 374$. As plotted in Fig. 5, there can be observed a positive correlation between the magnetic susceptibility of the nodules and the sediments from which they were extracted. It should be noted that the vivianite nodules never yield susceptibility below $0.8 \times 10^{-6}\,m^3\,kg^{-1}$, although the sediments can have much lower susceptibilities. Over half of the nodules measured come from sediment with low ($< 1.0 \times 10^{-6}\,m^3\,kg^{-1}$) susceptibility.

4.4 Field variation of susceptibility

Four nodule samples, all from zones of low susceptibility, were measured for susceptibility in a range of magnetic fields from 5 to 700 mA (Fig. 6). There is considerable scatter in the measurements at low fields ($< 100\,A\,m^{-1}$), probably due to relatively high measuring error at the very low fields (Hrouda et al., 2006) when dealing with paramagnetic material. Above $100\,A\,m^{-1}$ three of the samples show very little change in susceptibility, less than a few percent, whereas one sample (EV296) shows a consistent susceptibility but some 10 % higher than the original value.

CPD
8, 4989–5027, 2012

4.5 High temperature dependence of magnetic susceptibility

Selected nodule samples were continuously measured for susceptibility as the temperature was raised from room temperature to 700 °C and cycled back to 50 °C in air, with repeated cycles on the same samples (Fig. 7). The behavior of the nodules can be broken down into three general classes: those with heating and cooling curves that are not reversible and producing phases other than magnetite, those with non-reversible curves, but producing only magnetite, and curves that are nearly reversible.

4.5.1 Non-reversible curves with other phases than magnetite

In these samples the heating and cooling curves are not reversible during cycling to 700 °C. On initial heating low susceptibility is measured until 500 °C when there is increase of susceptibility with a marked peak occurring at about 560–570 °C, followed by a sharp drop at the Curie point of magnetite (Fig. 7a). The cooling curve displays a strong increase in susceptibility from the Curie temperature of magnetite to 500 °C followed by a continuous decrease. After the first heating run the susceptibility approximately doubled, suggesting the formation of magnetite within the vivianite sample. The heating curves of second run displays an increase in susceptibility at 330–350 °C and a sharp drop at 630 °C (Fig. 7a). The cooling curves are much higher than the heating curves, with a sharp increase in susceptibility from 630 °C reaching a maximum at temperatures of 280–330 °C, before a rapid decrease to room temperature. Heating and cooling curves of third runs are almost reversible and have same shape as cooling curves of second run but sharp drop of susceptibility on heating is not complete until 650 °C. Hysteresis data collected after each cycle is shown in Fig. 7b and tabulated in Table 4. The samples shows relatively high values for coercive force, H_c = 20–74 mA and coercivity of remanence, H_{cr} = 56–91 mA (corrected for paramagnetism) suggesting the formation a higher temperature magnetic phase.

CPD
8, 4989–5027, 2012

4.5.2 Non reversible curves producing magnetite

In these samples the heating and cooling curves are not reversible (Fig. 7c). *k*-*T* warming curves shows a gradual decrease in susceptibility and a sharp drop close to 580 °C marking a presence of magnetite. The cooling curves display a strong increase in susceptibility at the Curie temperature of magnetite, with a small but steady increase after 525 °C. After the first heating cycle, the susceptibility shows an increase 1.4 times the original. The heating curves of second run are similar as for 1st type curve and display an increase in susceptibility at 330–350 °C and a sharp drop at 615 °C. In the cooling path there is a marked increase in susceptibility starting at 615° C and reaching a maximum at 320 °C (Fig. 7c). On continued cooling the susceptibility makes a sharp drop before leveling off at a value nearly double the initial susceptibility. Hysteresis behavior after the first heating is shown in Fig. 7d, along with hysteresis parameters listed in Table 4. Ratios of J_{rs} to J_i and H_{cr} to H_c plot within the pseudo-single-domain field of Day et al. (1977).

4.5.3 Nearly reversible curves

In the samples shown in Fig. 7e the initial heating and cooling curves are almost reversible. There is a decrease in susceptibility up to 700 °C, with a cooling curve that is slightly lower but not markedly different. Susceptibility here includes up to 85 % due to a paramagnetic component, producing a noisy curve. Curie points of neither magnetite nor hematite are clearly visible on the graph. The heating curve for the second run is very similar to the first cooling curve. But, a marked change is observed in the second cooling run, with a strong increase in susceptibility observed at 620 °C, reaching its maximum at 270 °C, followed by a sharp decrease (Fig. 7e). Hysteresis behaviors after the first and second runs are plotted in Fig. 7f. There are moderate increases in H_c and H_{cr} from the first heating run to the second run (Table 4). The H_{cr}/H_c and J_{rs}/J_i ratios after second heating suggest formation of multi-domain magnetic phase.

CPD
8, 4989–5027, 2012

4.6 Saturation magnetization versus temperature

Additional material from the three samples discussed above was also studied for the behavior of magnetization (J_s) with heating to 700 °C (Fig. 8). The initial heating curve for each sample shows a small but distinctive "hump" marked by a slight increase in J_s at temperature 180–200 °C and a decrease at 320–340 °C. There is additionally a slight hint of a minor increase in J_s at 580 °C (Fig. 8). The second set of heating curves shows no hump, but continuous decay of the magnetization with increased temperature to 580 °C after which the curves appear to flatten out.

In comparing the high temperatures curves of magnetic susceptibility (Fig. 7a, c, e) to the saturation magnetization (Fig. 8a–c), several differences are noted. The visible increase in susceptibility at 500 °C for sample EV294 (Fig. 7a) is not observed on the J_s heating curve (Fig. 8a); the hump visible on all the initial curves of magnetization with temperature (Fig. 8) are no where evident on initial heating curves of susceptibility (Fig. 7).

4.7 High temperature behavior of vivianite with additive material

To further investigate the behavior of the vivianite nodules with other common materials in lake sediments, we studied high temperature susceptibility of vivianite mixed with various powders, as described by Minyuk et al. (2011). Powder from several vivianite nodules were mixed with sucrose (organic carbon), carbamide (nitrogen compound $(NH_2)_2CO$), metallic powder of arsenic, and elemental sulfur, with the additives never being more then 5 % of the total material. Samples were then heated continuously from room temperature to 700 °C and cooled back to room temperature.

No difference is seen in the heating and cooling curves for crushed vivianite samples without additive and those with sucrose or carbamide added (Fig. 9a–c). All the heating curves show small but distinct drops near 580 °C. Cooling curves all show a considerable increase in susceptibility starting at 580 °C, with continued increase to sharp peaks around 500 °C and then decay as the temperature decrease for the plain vivianite and

CPD
8, 4989–5027, 2012

the vivianite plus carbamide samples. The vivianite and sucrose sample also increases below 580 °C but continues to increase up to room temperature. All samples finish with susceptibility 1.5 to 2 times greater than the initial value.

A vivianite sample representative of first type *k-T* non-reversible curves was heated with arsenic. The initial vivianite run (Fig. 9d) has a large increase in susceptibility between 500–600 °C, indicating the formation of magnetite. When heated with arsenic this increase is not seen, although there a small increase occurred at lower temperature around 400 °C (Fig. 9e). It appears that the arsenic suppresses the formation of magnetite prior to the Curie temperature. The cooling curve for the arsenic-added sample does form magnetite at 580 °C and shows a steep increase to 450–500 °C as seen in the previous examples. A similar result of arsenic suppressing magnetite formation can be observed in the heating curves of plain chalcopyrite and chalcopyrite with arsenic (Fig. 9f).

There is a noticeable increase in susceptibility at 150–170 °C on the heating curves of vivianite with added sulfur (Fig. 9g). On cooling, increases in susceptibility are seen at Curie temperature of magnetite and monoclinic pyrrhotite. Heating the vivianite and sulfur mixture to temperatures of 200, 400 and 600 °C and cooling each time, shows that all heating and cooling curves are irreversible (Fig. 9h). The formation of pyrrhotite is seen only after the final 600 °C heating-cooling run. On all these runs the final susceptibility increases but always less than a factor of 2.

There are very different heating results when sulfur is added to goethite or hematite (Fig. 10b, e). After heating hematite and goethite with sulfur susceptibility increases between 400 and 610 times. The newly formed mineral is magnetite, indicated by the large increase in susceptibility at 580 °C.

Mixtures of vivianite and either hematite or goethite show vivianite to play the same reducing role that sulfur does. Heating a hematite and vivianite mixture (1 : 1) shows that during heating magnetite is formed (Fig. 10c). On cooling the susceptibility curve sharply increases at both 685 °C and 580 °C producing marked Hopkinson peaks for magnetite and hematite. The final magnetic susceptibility increases four-fold after the

CPD
8, 4989–5027, 2012

heating and cooling cycle. Goethite-vivianite mixture shows same cooling curves as for pure goethite, but without visible goethite-hematite transition at temperature 360 °C on heating curves (Fig. 10f). There is a small increase in susceptibility at 470 °C and the expected large drop at 580 °C. On cooling both the 580° C and 360 °C increases are noted, with final susceptibility again being four-fold larger than the initial.

Mixtures of pyrite and vivianite were also tested to further investigate changes in oxide mineralogy. The *k*-*T* curve of pyrite (Fig. 11a) is very similar to the heating and cooling curves of a 1 : 1 mixture of vivianite and pyrite (Fig. 11b). Very similar curves are also obtained when the mixture is 1 : 5 (Fig. 11c). In this case the Hopkinson peaks of monoclinic pyrrhotite are higher then magnetite ones. Cooling curves of mixture 1 : 10 are different, with no sharp increase in susceptibility at monoclinic pyrrhotite Curie temperature obvious (Fig. 11d). Susceptibility gradually increases from 600 to 280 °C on cooling, but on a second run heating curve there is a decrease in susceptibility at Curie temperature of monoclinic pyrrhotite. Distinct Hopkinson peaks of magnetite are observed on all curves of second runs.

k-*T* curves of mixture 1 : 50 yield another set of very different results (Fig. 11e). On cooling of the first run, susceptibility increases at 280 °C; the same increase is seen on the cooling curve of second run. Such increase suggests a formation of hexagonal pyrrhotite during cooling. During the second heating run the hexagonal pyrrhotite transfer to monoclinic pyrrhotite showing increase susceptibility at 220 °C and drop at 300–320 °C (Fig. 11e). This may reflect the so-called λ-transition from antiferro- to ferrimagnetic behavior as described by Dekkers (1989b) and Kontny et al. (2000). On the cooling curves of both runs is no visible increase in susceptibility at the Curie temperature of monoclinic pyrrhotite. Sharp magnetite Hopkinson peaks are evident on the heating and cooling curves of the second runs.

CPD
8, 4989–5027, 2012

5 Discussion

In El'gygytgyn Lake sediment vivianite is the more abundant authigenic mineral among other iron-bearing minerals such as pyrite, greigite, siderite, and Fe-Mn aggregates. The nodules and concretions of vivianite occur that along the core profile amount to few gram per sample (weight of sample is 6 g in average). Morphological features of nodules are variable suggesting different growth conditions. Some nodules are empty or filled with crystals in central parts indicating growth of the concretions from the surface towards center. Other nodules consist of crystal clusters with randomly oriented fragile crystals suggesting that nodules formed before sediment compaction.

Magnetic behavior of vivianite particles and nodules is important to overall interpretation of magnetic properties of lacustrine sediments that are used as environmental proxies. In the study of Lake El'gygytgyn, magnetic susceptibility is an important parameter, and is used for core descriptions, correlations and dating (Melles et al., 2012; Nowaczyk et al., 2007, 2012). Vivianite is paramagnetic at room temperature and becomes antiferromagnetic (weakly magnetic) only at low temperatures (< 20 K). But, samples studied here show that the nodules have magnetic susceptibility similar to many of the lake sediments, and often higher than the susceptibility of sediments from the cold intervals. In that case vivianite may obscure the environmental signal of rock magnetic properties of the bulk sediment. For example, magnetic susceptibility in general shows low values in stage 6 but at depths 7.05–7.26 m and 9.13–9.33 m magnetic susceptibility has increased (Fig. 3). Simultaneously, this depth is enriched in P_2O_5 and MnO that may enhance the formation of vivianite. Correlation coefficients between P_2O_5 and magnetic susceptibility in intervals 7.05–7.26 m and 9.13–9.33 m are 0.47 and 0.68, respectively. In stage 7.4 at depth 11.59–12.19 m the high P_2O_5 content positively correlates with increased MS values ($r = 0.58$) indicating fine grained vivianite is also present. Large vivianite nodules are absent in Fe-P-Mn intervals suggesting precipitation of vivianite directly from lake water that can be related to events of climate and environmental change.

CPD
8, 4989–5027, 2012

In most cases, the vivianite concretions are not homogeneous, but contain irregular oxidized patches. In backscattered electron images the oxidized parts have lighter color and record higher Fe and P content (Fig. 4a, b). The oxidized parts are often located along cracks and in outer parts of nodule grains, and possibly consist of metavivianite or santabarbaraite. Some oxidation spots are depleted in Mn as was reported by Fagel et al. (2005) for Baikal vivianite. On the other hand, Pratt (1997) indicates that the product of vivianite auto-oxidation on cleaved surfaces is ferric hydroxide. Sapota et al. (2006) indicate that some Baikal vivianite microconcretions are covered with yellow-brown iron oxides, likely goethite. In a calcareous medium vivianite is oxidized to poorly crystalline lepidocrocite (Roldán et al., 2002).

However, the products of oxidation appear to have little influence on the magnetic properties of vivianite due to the weak magnetic susceptibility of any of the oxidation products.

Lepidocrocite is paramagnetic at room temperature with a low field susceptibility of $57.8 \times 10^{-8}\,m^3\,kg^{-1}$ (e.g. Hirt et al., 2002), goethite is antiferromagnetic with susceptibility $0.5–1.5 \times 10^{-6}\,m^3\,kg^{-1}$ (e.g. Dekkers, 1989a). Magnetic susceptibility of nodules ($n = 54$) exhibit values between $0.78 \times 10^{-6}\,m^3\,kg^{-1}$ and $1.72 \times 10^{-6}\,m^3\,kg^{-1}$ (average $= 1.05 \times 10^{-6}\,m^3\,kg^{-1}$). Numerous nodules include grains of sulphides, ilmenite, iron, titanomagnetite, and/or clay minerals. Some magnetic inclusions could increase the attraction of nodules to a magnet and, thus, increase magnetic susceptibility. Positive correlation between magnetic susceptibility of nodules and magnetic susceptibility of sediment suggest that during growth the nodules capture grains from sediments. But this included material is a secondary source of magnetic susceptibility because the susceptibility of the nodules is higher than that of the sediment from low magnetic intervals.

Investigations of behavior of vivianite upon cyclic heating and cooling reveal the mineralogical changes that can occur in this system. The formation of new mineral phases, predominantly magnetite and/or hematite, occurs when vivianite samples are repeatedly heated and cooled to 700 °C .

CPD
8, 4989–5027, 2012

There are three types of *k*-*T* curves (Fig. 7). The characteristic features of all vivianite nodules are observed in the cooling curves of second and third runs. These curves show an increase in susceptibility from 620–650 °C to 250–300 °C followed by a sharp drop.

J_s-*T* curves show increased J_s during heating at temperatures from 180–200 °C (Fig. 8). The hump on the curves possibly reflects the dehydration of vivianite and the ensuing oxidation Fe^{2+}.

Natural vivianite shows weight loss steps at 105, 138, 203, 272 and 437 °C that are attributed to dehydration (Frost et al., 2003). Marincea et al. (1997) point out that endothermic peaks recorded on the differential thermal analysis DTA curve at temperature 183 °C and 205 °C marks a major loss of structurally bound H_2O and beginning of oxidation of Fe^{2+} to Fe^{3+}. The exothermic peak recorded on the DTA curve at 270 °C corresponds to another phase of oxidation. Rodgers and Henderson (1986) report the loss of structural water combined with the oxidation of Fe^{2+} spanning 65 to 315 °C, and the formation of a-$FePO_4$, $Fe(PO_3)_3$ and, occasionally, Fe_2O_3, as marked on DTA curve at 660° C. On *k*-*T* curves there are no visible signs of dehydration of vivianite at these temperatures indicating that this process does not influence magnetic susceptibility.

k-*T* curves of first type show increased susceptibility on heating at temperature 500 °C (Fig. 7a). The hump on heating curves is possible attributed to the transformation of sulfides from pyrite to magnetite during heating. But pyrite transformation during heating usually begins at temperatures of 420–450 °C, and forms magnetite and monoclinic pyrrhotite (e.g. Wang et al., 2008; Tanikawa et al., 2008). Thermomagnetic study of vivianite and pyrite mixtures show that depending on the mixture composition produce monoclinic or hexagonal pyrrhotite (Fig. 11). In our case monoclinic pyrrhotite (high pyrite content) or hexagonal pyrite (low pyrite content) do not form.

A plausible explanation can be obtained with goethite as an oxidation product of vivianite. Goethite shows no such hump on heating curves (Fig. 10d) but on heating a mixture of vivianite and goethite a similar increase in susceptibility is seen after 500 °C (Fig. 10f).

CPD
8, 4989–5027, 2012

Continued cycling of samples from the first type shows in the second run a phase formed at ~620 °C. On the third run it has increased to 650 °C. If this is indicative of a Curie temperature (630–650 °C), it is lower then hematite and closer to maghemite (Özdemir, 1990; Gehring et al., 2009). According to J_{rs}/J_i and H_{cr}/H_c ratios the single domain particles were formed during the first heating (Day et al., 1977). The decrease of H_c and H_{cr} after few cycles of heating and cooling, a decrease in J_{rs}/J_i, and an increase in H_{cr}/H_c indicate the formation of lower coercivity minerals and larger domain state particles (Table 4, sample EV294).

Thermomagnetic data shows that quantities of magnetic minerals are not generated during heating and cooling. Magnetic susceptibility does not increase by more than twofold after heating.

The behavior of the susceptibility of vivianite upon heating in different media was monitored. Vivianite mixed with sucrose (organic carbon) or carbamide (nitrogen) shows similar thermomagnetic curves as vivianite without the additive. Arsenic suppresses the generation of magnetite at temperatures lower than the Curie temperature of this mineral (578 °C). But, magnetite that formed at higher temperature is the same amount as that formed after heating vivianite with sucrose and carbamide. Specific thermomagnetic curves are produced for vivianite mixed with elemental sulfur. All first heating curves show a small hump in susceptibility at temperatures of 150–170 °C. Interpretation of this hump is highly ambiguous. Such increase in susceptibility may reflect λ-transition from antiferro- to ferrimagnetic behavior of pyrrhotite. Kontny at al. (2000) report temperatures of 160–210 °C for this transition. According to Li and Franzen (1996) thermomagnetic heating-cooling curves for a peak-type pyrrhotite in the temperature range between 20 and 400 °C are reversed from this. Our data indicates that the mineral phase formed here is unstable. *k-T* curves after heating to 200 °C and to 400 °C exhibit irreversible thermomagnetic behaviors (Fig. 9h). After heating the sulfur-vivianite mixture to 600 °C, monoclinic pyrrhotite, marked by Hopkinson peak on cooling curve at temperature 320 °C, are formed. Such behavior is different from

CPD
8, 4989–5027, 2012

thermomagnetic curves of hematite and goethite mixtures with sulfur showing formation of magnetite in large amounts (Fig. 10b, e).

Thermomagnetic data are widely used to diagnostic magnetic minerals but heating media and the presence of other minerals in the samples can complicate interpretation of the results. The influence of vivianite on the thermomagnetic behavior of hematite, goethite and pyrite was investigated. Hematite-vivianite mixture (1 : 1) shows that vivianite acts as a reductant and stimulates formation of magnetite (Fig. 10c). During heating of goethite-vivianite mixture (1 : 1) the vivianite suppresses the goethite-hematite transition but stimulates formation of magnetite (Fig. 10f). Behavior of a pyrite and vivianite mixture during heating depends on the specific pyrite/vivianite content. Thermomagnetic curves for mixture with vivianite content up to 80 % are nearly similar to those for pyrite (Fig. 11a–c). Pyrite/vivianite mixing ratio 1 : 10 show formation of magnetite and monoclinic pyrrhotite during heating but lacking the sharp Hopkinson peak of pyrrhotite on cooling. A second heating run produces more magnetite. Heating-cooling of a pyrite/vivianite mixture (1 : 50) exhibits the formation of hexagonal pyrrhotite. This pyrrhotite is unstable during a second heating and transforms to unstable monoclinic pyrrhotite and magnetite, as seen on the cooling curve of the second run.

6 Conclusions

Vivianite nodules are abundant in both sediments of cold (anoxic) and warm (oxic) stages. Magnetic susceptibility of vivianite nodules varies from $0.78 \times 10^{-6}\,m^3\,kg^{-1}$ to $1.72 \times 10^{-6}\,m^3\,kg^{-1}$ (average = $1.05 \times 10^{-6}\,m^3\,kg^{-1}$) and is higher than the susceptibility of sediments from the cold intervals. This susceptibility of vivianite can then obscure the environmental signal determined from rock magnetic properties.

Magnetic properties of vivianite are due to product of oxidation as well as sediment and mineral inclusions.

CPD
8, 4989–5027, 2012

There are three types of curves of high temperature versus susceptibility for vivianite indicating different degrees of oxidation and inclusions in nodules.

Vivianite act as a reductant and reduces hematite to magnetite, while also inhibiting the goethite-hematite transition during heating.

Adding sulfur to vivianite stimulates formation of monoclinic pyrrhotite, whereas the addition of arsenic suppresses the formation of magnetite below its Curie temperature.

Heating selective vivianite and pyrite mixtures shows formation of different minerals – magnetite, monoclinic pyrrhotite, and hexagonal pyrrhotite that make it difficult to interpret the thermomagnetic curves.

Acknowledgements. Drilling operations were funded by the ICDP, the NSF, the German Federal Ministry of Education and Research (BMBF), Alfred Wegener Institute and Helmholtz Centre Potsdam (GFZ), Far East Branch of the Russian Academy of Sciences (FEB RAS), the Russian Foundation for Basic Research (RFBR), and the Austrian Federal Ministry of Science and Research. The Russian Global Lake Drilling 800 drilling system was developed and operated by DOSECC. Funding of sample analyses was provided by the Civilian Research and Development Foundation (grant RUG1-2987-MA-10), RFBR (grant 12-05-00286), FEB RAS (12-II-SB-08-024; 12-III-A-08-191; 12-III-V-08-191).

References

Asikainen, C. A., Francus, P., and Brigham-Grette, J.: Sedimentology, clay mineralogy and grain-size as indicators of 65 ka of climate change from El'gygytgyn Crater lake, Northeastern Siberia, J. Paleolimnol., 37, 105–122, 2007.

Bassinot, F. C., Labeyrie, L. D., Vincent, E., Quidelleur, X., Shackleton, N. J., and Lancelot, Y.: The astronomical theory of climate and the age of the Brunhes-Matuyama magnetic reversal, Earth Planet. Sc. Lett, 126, 91–108, 1994.

Bely, V. F. and Belaya, B. V.: Late Stage of the OCVB Development (Upstream of the Enmyvaam River), NEISRI FEB RAS Press, Magadan, 1998 (in Russian).

Bely, V. F. and Raikevich, M. I.: The El'gygytgyn Lake Basin (Geological Structure, Morphostructure, Impactites, Problems of Investigation and Preservation of Nature), NEISRI FEB RAS Press, Magadan, 1994 (in Russian).

CPD
8, 4989–5027, 2012

Borkhodoev, V. Y.: Accuracy of the fundamental parameter method for X-ray fluorescence analysis of rocks, X-Ray Spectrom., 31, 209–218, 2002.
Brigham-Grette, J., Melles, M., Minyuk, P., and Scientific Party: Overview and significance of a 250 ka paleoclimate record from El'gygytgyn Crater Lake, NE Russia, J. Paleolimnol., 37, 1–16, 2007.
Burov, B. V., Nourgaliev, D. K., and Yasonov, P. G.: Paleomagnetic Analysis, KGU Press, Kazan, 1986 (in Russian).
Day, R., Fuller, M., and Schmidt, V. A.: Hysteresis properties of titanomagnetites: grain size and composition dependence, Phys. Earth Planet. Int., 13, 260–267, 1977.
Dekkers, M. J.: Magnetic properties of natural goethite – I. Grain-size dependence of some low- and high-field related rockmagnetic parameters measured at room temperature, Geophys. J., 97, 323–340, 1989a.
Dekkers, M. J.: Magnetic properties of natural pyrrhotite – II. High- and low-temperature behavior of Jrs and TRM as function of grain size, Phys. Earth Planet. Int., 57, 266–283, 1989b.
Fagel, N., Alleman, L. Y., Granina, L., Hatert, F., Thamo-Bozso, E., Cloots, R., and Andre, L.: Vivianite formation and distribution in Lake Baikal sediments, Global Planet. Change, 46, 315–336, 2005.
Frederichs, T., von Dobeneck, T., Bleil, U., and Dekkers, M. J.: Towards the identification of siderite, rhodochrosite, and vivianite in sediments by their low-temperature magnetic properties, Phys. Chem. Earth, 28, 669–679, 2003.
Frost, R. L., Weier, M. L., Martens, W., Kloprogge, J. T., and Ding, Z.: Dehydration of synthetic and natural vivianite, Thermochim. Acta, 401, 121–130, 2003.
Gehring, A. U., Fischer, H., Louvel, M., Kunze, K., and Weidler, P. G.: High temperature stability of natural maghemite: a magnetic and spectroscopic study, Geophys. J. Int., 179, 1361–1371, 2009.
Gurov, E. P., Koerbel, C., and Yamnichenko, A.: El'gygytgyn impact crater, Russia: structure, tectonics, and morphology, Meteorit. Planet. Sci., 42, 307–319, 2007.
Hirt, A. M., Lanci, L., Dobson, J., Weidler, P., and Gehring, A. U.: Low-temperature magnetic properties of lepidocrocite, J. Geophys. Res., 107, 2011, doi:10.1029/2001JB000242, 2002.
Hrouda, F., Chlupacova, M., and Mrazova, S.: Low-field variation of magnetic susceptibility as a tool for magnetic mineralogy of rocks, Phys. Earth Planet. Int., 154, 323–336, 2006.

CPD
8, 4989–5027, 2012

Kontny, A., De Wall, H., Sharp, T. G., and Posfai, M.: Mineralogy and magnetic behavior of pyrrhotite from a 260 °C section at the KTB drilling site, Germany, Am. Mineral., 85, 1416–1427, 2000.
Layer, P.: Argon-40/argon-39 age of the El'gygytgyn impact event, Chukotka, Russia, Meteorit. Planet. Sci., 35, 591–599, 2000.
Li, F. and Franzen, H. F.: Ordering, incommensuration, and phase transitions in pyrrhotite. Part II: A high-temperature X-ray powder diffraction and thermomagnetic study, J. Solid State Chem., 126, 108–120, 1996.
Manning, P. G., Murphy, T. P., and Prepas, E. E.: Intensive formation of vivianite in the bottom sediments of mesotrophic Narrow Lake, Alberta, Can. Mineral., 29, 77–85, 1991.
Manning, P. G., Prepas, E. E., and Serediak, M. S.: Pyrite and vivianite intervals in the bottom sediments of eutrophic Baptiste Lake, Alberta, Canada, Can. Mineral., 37, 593–601, 1999.
Marincea, S., Constantinescu, E., and Ladriere, J.: Relatively unoxidized vivianite in limnic coal from Capeni Baraolt Basin, Romania, Can. Mineral., 35, 713–722, 1997.
Meijer, H. C., van den Handel, J., and Frikkee, E.: Magnetic behavior of vivianite, $Fe_3(PO_4)_2 \cdot 8H_2O$, Physica, 34, 475–48, 1967.
Melles, M., Brigham-Grette, J., Glushkova, O. Yu., Minyuk, P., Nowaczyk, N., and Hubberten, W.: Sedimentary geochemistry of a pilot core from Lake El'gygytgyn – a sensitive record of climate variability in the East Siberian Arctic during the past three climate cycles, J. Paleolimnol., 37, 89–104, 2007.
Melles, M., Brigham-Grette, J., Minyuk, P., Koeberl, C., Andreev, A., Cook, T., Fedorov, G., Gebhardt, C., Haltia-Hovi, E., Kukkonen, M., Nowaczyk, N., Schwamborn, G., Wennrich, V., and the El'gygytgyn Scientific Party: The Lake El'gygytgyn scientific drilling project – conquering Arctic challenges through continental drilling, Scientific Drilling, 11, 29–40, 2011.
Melles, M., Brigham-Grette, J., Minyuk, P. S., Nowaczyk, N. R., Wennrich, V., DeConto, R. M., Anderson, P. M., Andreev, A. A., Coletti, A., Cook, T. L., Haltia-Hovi, E., Kukkonen, M., Lozhkin, A. V., Rosén, P., Tarasov, P., Vogel, H., Wagner, B.: 2.8 million years of Arctic climate change from Lake El'gygytgyn, NE Russia, Science, 337, 315–320, 2012.
Minyuk, P. S., Brigham-Grette, J., Melles, M., Borkhodoev, V. Y., and Glushkova, O. Y.: Inorganic geochemistry of El'gygytgyn Lake sediments (Northeastern Russia) as an indicator of paleoclimatic change for the last 250 kyr, J. Paleolimnol., 37, 123–133, 2007.
Minyuk, P. S., Subbotnikova, T. V., and Plyashkevich, A. A.: Measurements of thermal magnetic susceptibility of hematite and goethite, Izvestia, Phys. Solid Earth, 47, 762–774, 2011.

CPD
8, 4989–5027, 2012

Murdock, K. J., Wilkie, K. M., and Brown, L. L.: Rock magnetic properties, magnetic susceptibility, and organic geochemistry comparison in core LZ1029-7 Lake El'gygytgyn, Far Eastern Russia, Clim. Past Discuss., 8, 4565–4599, doi:10.5194/cpd-8-4565-2012, 2012.
Nembrin, G. P., Capobianco, J. A., Viel, M., and Williams, A. F.: A Mössbauer and chemical study of the formation of vivianite in sediments of Lago Maggiore (Italy), Geochim. Cosmochim. Acta, 47, 1459–1464, 1983.
Nolan, M. and Brigham-Grette, J.: Basic hydrology, limnology, and meterology of modern Lake El'gygytgyn, Siberia, J. Paleolimnol., 37, 17–35, 2007.
Nowaczyk, N. R., Melles, M., and Minyuk, P.: A revised age model for core PG1351 from Lake El'gygytgyn, Chukotka, based on magnetic susceptibility variations tuned to Northern Hemisphere insolation variations, J. Paleolimnol., 37, 65–76, 2007.
Nowaczyk, N. R., Haltia-Hovi, E. M., Ulbricht, D., Wennrich, V., Kukkonen, M., Rosen, P., Vogel, H., Meyer-Jacob, C., Andreev, A., Lozhkin, A. V., and El'gygytgyn Scientific Party: Chronology of Lake El'gygytgyn sediments, Clim. Past, submitted, 2012.
Nriagu, J. O. and Dell, C. I.: Diagenetic formation of iron phosphates in recent lake sediments, Am. Mineral., 59, 934–946, 1974.
Özdemir, Ö.: High-temperature hysteresis and thermoremanence of single-domain maghemite, Phys. Earth Planet. Int., 65, 125–136, 1990.
Pratesi, G., Cipriani, C., Guili, G., and Birch, W. D.: Santabarbaraite: a new amorphous phosphate mineral, Eur. J. Mineral., 15, 185–192, 2003.
Pratt, A. R.: Vivianite auto-oxidation, Phys. Chem. Mineral., 25, 24–27, 1997
Rodgers, K. A.: Metavivianite and kerchenite: a review, Mineral. Mag., 50, 687–691, 1986.
Rodgers, K. A. and Henderson, G. S.: The thermochemistry of some iron phosphate minerals: vivianite, metavivianite, baracite, ludlamite and vivianite/metavivianite admixtures, Thermochim. Acta, 104, 1–12, 1986.
Roldán, R., Barrón, V., and Torrent, J.: Experimental alteration of vivianite to lepidocrocite in a calcareous medium, Clay Miner., 37, 709–718, 2002.
Rosenquist, I. T.: Formation of vivianite in Holocene clay sediments, Lithos, 3, 327–334, 1970.
Sapota, T., Aldahan, A., and Al-Aasm, I. S.: Sedimentary facies and climate control on formation of vivianite and siderite microconcretions in sediments of Lake Baikal, Siberia, J. Paleolimnol., 36, 245–257, 2006.

CPD
8, 4989–5027, 2012

Tanikawa, W., Mishima, T., Hirono, T., Soh, W., and Song, S. R.: High magnetic susceptibility produced by thermal decomposition of core samples from the Chelungpu fault in Taiwan, Earth Planet. Sc. Lett., 272, 372–381, 2008.
Wang, L., Pan, Y., Li, J., and Qin, H.: Magnetic properties related to thermal treatment of pyrite, Sci. China. Ser. D, 5, 1144–1153, 2008.

CPD
8, 4989–5027, 2012

Table 1. Electron-microprobe analyses of selected vivianite nodules from El'gygytgyn Lake.

Nodule	Analyze	P_2O_5 %	Fe_2O_3 %	MnO %	P %	Fe %	Mn %	P normalised wt %	Fe	Mn	P/Mn wt/wt
10	1	27.61	39.4	1.85	12.06	30.54	1.43	40.46	56.83	2.71	14.93
	2	21.23	34.01	2.22	9.27	26.36	1.72	37.29	58.81	3.90	9.562
	3	27.80	37.64	2.01	12.14	29.18	1.56	41.58	55.42	3.01	13.81
	4	25.37	37.57	1.33	11.08	29.12	1.03	39.84	58.07	2.09	19.06
9	5	26.39	37.37	1.22	11.52	28.97	0.95	40.98	57.12	1.90	21.57
	6	25.07	39.24	0.67	10.95	30.42	0.52	38.95	60.01	1.04	37.45
	7	22.07	37.18	1.02	9.64	28.82	0.79	36.97	61.32	1.71	21.62
	8	25.78	35.96	1.46	11.26	27.88	1.13	41.16	56.51	2.33	17.67
8	9	25.95	33.99	4.31	11.33	26.35	3.34	40.72	52.51	6.77	6.01
	12	29.28	34.03	6.34	12.79	26.38	4.91	42.36	48.46	9.18	4.61
7	13	26.46	36.11	1.92	11.55	27.99	1.49	41.39	55.60	3.00	13.80
	14	27.91	36.18	1.31	12.19	28.05	1.02	43.05	54.93	2.02	21.31
	15	23.08	31.74	2.15	10.08	24.60	1.67	40.87	55.32	3.81	10.73
	16	25.49	36.88	1.93	11.13	28.59	1.50	40.00	56.97	3.03	13.20
6	17	22.7	34.61	1.62	9.91	26.83	1.26	38.88	58.35	2.78	13.99
	18	25.64	38.16	1.38	11.20	29.58	1.07	39.70	58.16	2.14	18.55
	19	26.93	36.44	1.11	11.76	28.25	0.86	42.14	56.13	1.74	24.22
	20	25.76	35.44	1.88	11.25	27.47	1.46	41.20	55.79	3.01	13.69
5	21	26.21	36.43	2.22	11.45	28.24	1.72	40.77	55.78	3.45	11.82
	22	25.27	35.43	1.84	11.03	27.47	1.43	40.77	56.26	2.97	13.73
	23	24.72	35.48	2.07	10.79	27.50	1.60	40.05	56.59	3.36	11.92
	24	26.41	33.83	4.36	11.53	26.22	3.38	41.22	51.97	6.81	6.05
4	25	25.58	36.00	3.61	11.17	27.91	2.80	39.58	54.83	5.59	7.08
	26	25.99	34.15	1.35	11.35	26.47	1.05	42.64	55.15	2.22	19.21
	27	23.48	34.61	2.20	10.25	26.83	1.71	39.30	57.02	3.68	10.68
	28	24.85	34.14	2.21	10.85	26.47	1.71	40.96	55.39	3.65	11.22
3	29	22.52	32.41	1.67	9.834	25.12	1.29	40.15	56.87	2.98	13.47
	30	22.83	34.13	1.23	9.969	26.46	0.95	39.60	58.27	2.13	18.59
	31	22.60	30.18	1.36	9.869	23.40	1.05	42.11	55.35	2.54	16.58
	32	22.16	32.10	2.55	9.677	24.88	1.98	39.35	56.12	4.53	8.69
2	33	22.43	32.87	2.15	9.795	25.48	1.67	39.39	56.83	3.78	10.42
	34	25.54	35.07	1.72	11.15	27.19	1.33	41.34	55.88	2.79	14.82
	35	23.26	34.33	2.71	10.16	26.61	2.10	38.92	56.54	4.54	8.57
	36	25.98	34.59	1.89	11.34	26.81	1.47	41.96	54.99	3.05	13.76
1	37	24.79	34.34	1.32	10.83	26.62	1.02	41.38	56.42	2.20	18.81
	38	25.52	34.28	1.58	11.14	26.57	1.22	41.94	55.46	2.60	16.13
	39	25.22	35.52	2.45	11.01	27.53	1.90	40.26	55.82	3.91	10.30

CPD
8, 4989–5027, 2012

Table 2. Chemical composition of P-Mn rich sediments intervals.

Depth, m	Fe_2O_3, % (average)	P_2O_5, % (average)	MnO, % (average)	P/Mn	Fe/P
8.71–9.21	6.33–8.97 (7.58)	0.20–0.88 (0.44)	0.08–0.45 (0.19)	0.58	0.72
11.51–12.19	5.61–8.99 (7.03)	0.12–1.94 (0.39)	0.07–0.55 (0.20)	0.59	0.66
13.19–13.51	6.03–7.74 (6.72)	0.09–1.18 (0.46)	0.07–0.12 (0.09)	0.98	0.87
18.39–18.85	2.54–5.99 (3.57)	0.06–2.32 (0.52)	0.05–0.36 (0.12)	0.93	0.92
20.95–21.17	4.48–7.74 (5.67)	0.06–1.92 (0.53)	0.05–0.22 (0.10)	0.99	0.96
24.31–24.73	3.96–6.77 (5.17)	0.07–0.88 (0.21)	0.05–0.13 (0.07)	0.90	0.42

CPD
8, 4989–5027, 2012

Table 3. Magnetic susceptibility of vivianite nodules.

Sample	Depth m	Weight, Nodules mg	MS, vivianite $10^{-6}\,m^3\,kg^{-1}$	MS, sediment $10^{-6}\,m^3\,kg^{-1}$	Magnetic interval
24	6.13	332	1.12	0.567	L
25	6.15	651	0.940	0.607	L
26	6.17	108	0.866	0.260	L
43	6.51	113	0.993	0.252	L
44	6.53	180	0.993	0.248	L
67	6.99	118	0.945	0.453	L
68	7.01	457	0.886	0.213	L
73	7.01	170	0.810	0.388	L
74	7.12	136	0.839	0.191	L
159	9.35	112	1.43	0.207	L
163	9.53	156	0.919	0.453	L
287	12.35	247	1.54	2.129	H
296	12.53	200	1.288	2.655	H
297	12.55	330	1.274	1.956	H
303	12.67	416	0.971	0.548	L
361	13.97	417	1.72	2.110	H
369	14.13	419	1.01	1.689	H
370	14.15	551	1.12	1.606	H
385	14.57	104	1.23	1.867	H
387	15.21	176	1.11	2.472	H
388	15.23	303	1.03	2.559	H
389	15.25	113	1.04	2.667	H
438	16.23	181	1.15	2.302	H
439	16.25	254	1.08	1.781	H
445	16.37	437	0.888	0.165	L
484	17.27	2363	0.960	1.410	H
485	17.29	1082	0.844	0.311	L
488	17.35	2854	0.787	0.171	L
597	19.59	598	0.868	0.405	L

CPD
8, 4989–5027, 2012

Table 3. Continued.

Sample	Depth m	Weight, Nodules mg	MS, vivianite $10^{-6}\,m^3\,kg^{-1}$	MS, sediment $10^{-6}\,m^3\,kg^{-1}$	Magnetic interval
620	20.05	214	1.34	1.533	H
621	20.07	109	1.09	0.851	H
622	20.09	1127	0.914	0.378	L
632	20.41	360	0.878	0.296	L
644	20.65	247	0.775	0.692	L
683	21.58	202	1.53	1.754	H
687	21.66	382	1.13	1.858	H
715	22.33	122	1.06	0.145	L
716	22.35	495	0.908	0.164	L
717	22.37	275	0.815	0.190	L
725	22.59	127	0.846	0.131	L
733	22.75	124	1.15	2.105	H
754	23.17	273	0.870	0.987	H
816	24.59	167	1.28	2.967	H
819	24.65	170	1.07	1.360	H
822	24.71	354	0.880	0.330	L
823	24.73	1198	0.915	0.472	L
844	25.34	145	1.44	1.937	H
845	25.36	155	1.20	2.253	H
846	25.38	117	1.28	2.192	H
853	25.52	165	0.927	0.222	L
854	25.54	623	0.865	0.215	L
855	25.56	404	0.881	0.400	L
877	26.00	198	1.03	3.141	H
878	26.02	213	1.43	2.252	H
901	26.55	124	0.782	0.163	L
937	27.37	207	1.08	1.199	H

L (H) – Low (high) susceptibility intervals.

CPD
8, 4989–5027, 2012

Table 4. Hysteresis parameters of vivianite nodules.

Sample	Depth, m	H_c (corrected)	H_{cr}	J_i (corrected)	J_{rs}	J_{rs}/J_i (corrected)	H_{cr}/H_c (corrected)
EV294	12.49	36.53 (74.07)	91.36	0.35 (0.02)	0.03	0.09 (1.11)	2.50 (1.23)
EV294							
1st heating		41.15 (50.32)	91.72	0.79 (0.37)	0.16	0.20 (0.44)	2.22 (1.82)
EV294							
2nd heating		20.02 (22.71)	62.72	1.05 (0.56)	0.17	0.16 (0.30)	3.13 (2.76)
EV294							
3rd heating		18.07 (20.03)	56.89	0.97 (0.50)	0.14	0.15 (0.29)	3.14 (2.83)
EV-297	12.55	26.34 (77.25)	90.81	0.37 (0.02)	0.02	0.05 (1.18)	3.44 (1.17)
EV297							
1st heating		23.56 (34.84)	75.79	0.57 (0.17)	0.05	0.10 (0.32)	3.21 (2.17)
EV297							
2nd heating		23.34 (31.24)	97.78	0.77 (0.28)	0.10	0.13 (0.36)	4.18 (3.13)
EV297+AS							
1st heating		35.22 (49.77)	93.60	0.65 (0.21)	0.09	0.14 (0.44)	2.65 (1.88)
EV297+S							
1st heating		46.48 (72.68)	149.30	0.55 (0.20)	0.08	0.14 (0.40)	3.21 (2.05)
EV297+S							
2nd heating		22.92 (25.53)	59.45	1.16 (0.69)	0.20	0.17 (0.29)	2.59 (2.32)
EV-622-1	20.09						
1st heating		3.33 (4.40)	68.01	0.36 (0.02)	0.002	0.01 (0.10)	–
EV-622-1							
2nd heating		12.79 (21.44)	107.24	0.39 (0.07)	0.01	0.02 (0.15)	8.38 (5.00)
EV687	21.66	11.12 (25.77)	63.75	0.36 (0.04)	0.01	0.02 (0.29)	5.72 (2.47)
EV687							
1st heating		14.67 (23.30)	73.64	0.52 (0.14)	0.03	0.06 (0.23)	5.01 (3.15)
EVSM	17.27–17.35	7.3 (27.46)	67.24	0.33 (0.02)	0.01	0.01 (0.27)	9.16 (2.44)
EVSM+S							
1st heating		72.24 (130.71)	168.87	0.50 (0.11)	0.10	0.19 (0.84)	2.33 (1.29)
EVSM+0							
1st heating		13.30 (23.59)	67.73	0.46 (0.09)	0.02	0.04 (0.25)	5.09 (2.87)
EVSM+N							
1st heating		36.81 (51.65)	102.98	0.65 (0.22)	0.09	0.14 (0.40)	2.79 (1.99)

In brackets – parameters corrected for paramagnetism.

CPD
8, 4989–5027, 2012

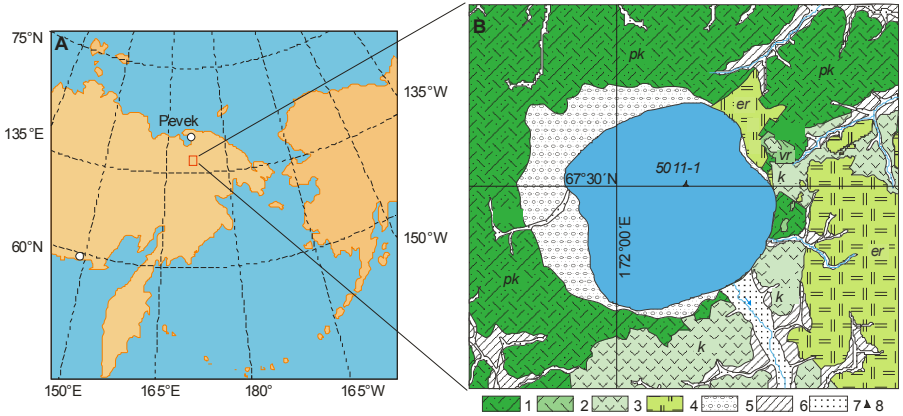

Fig. 1. (A) Location of Lake El'gygytgyn in easternmost Russia. **(B)** Simplified bedrock geologic map of the Lake El'gygytgyn adapted from Bely and Raikevich (1994); Bely and Belaya (1998). Formation: 1 – Pykarvaam (*pk*); 2 – Voronian (*vr*); 3 – Koekvun' (*k*); 4 – Ergyvaam (*er*); 5 – deluvian; 6 – terrace deposits; 7 – flood plain deposits; 8 – core site.

CPD
8, 4989–5027, 2012

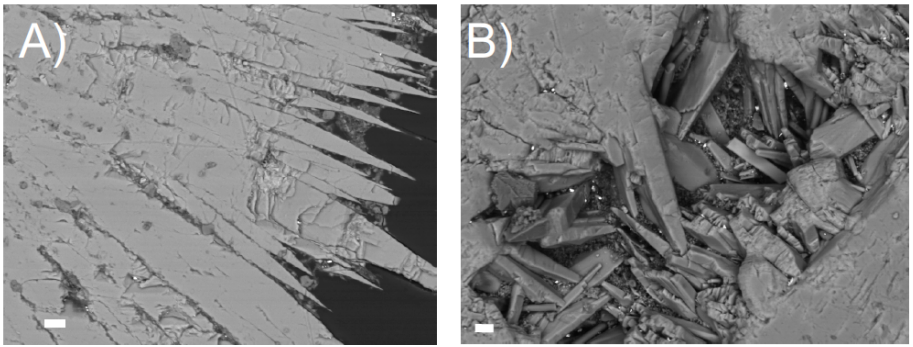

Fig. 2. Backscattered electron images of polished sections of vivianite microconcretions: **(A)** outer surface of a concretion, **(B)** inner part of a concretion with visible crystals. Scale (white line) is 20 µm.

CPD
8, 4989–5027, 2012

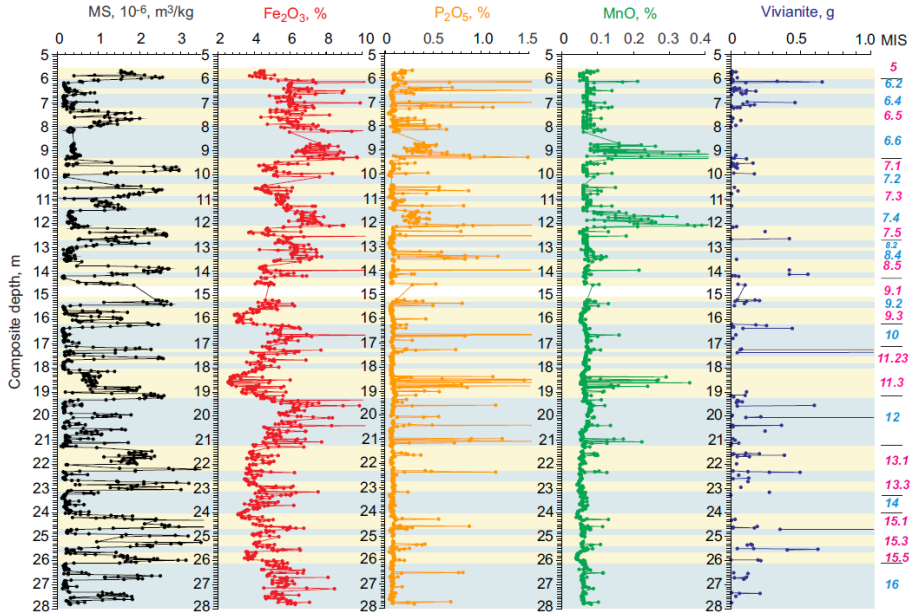

Fig. 3. Distribution of magnetic susceptibility (MS), percent Fe_2O_3, P_2O_5, and MnO, and occurrence of vivianite nodules, in grams, in sediments samples over 28 m of core material. Marine isotope stages (MIS) adapted from Bassinot et al. (1994). Blue (yellow) bars indicate cold (warm) stages.

CPD
8, 4989–5027, 2012

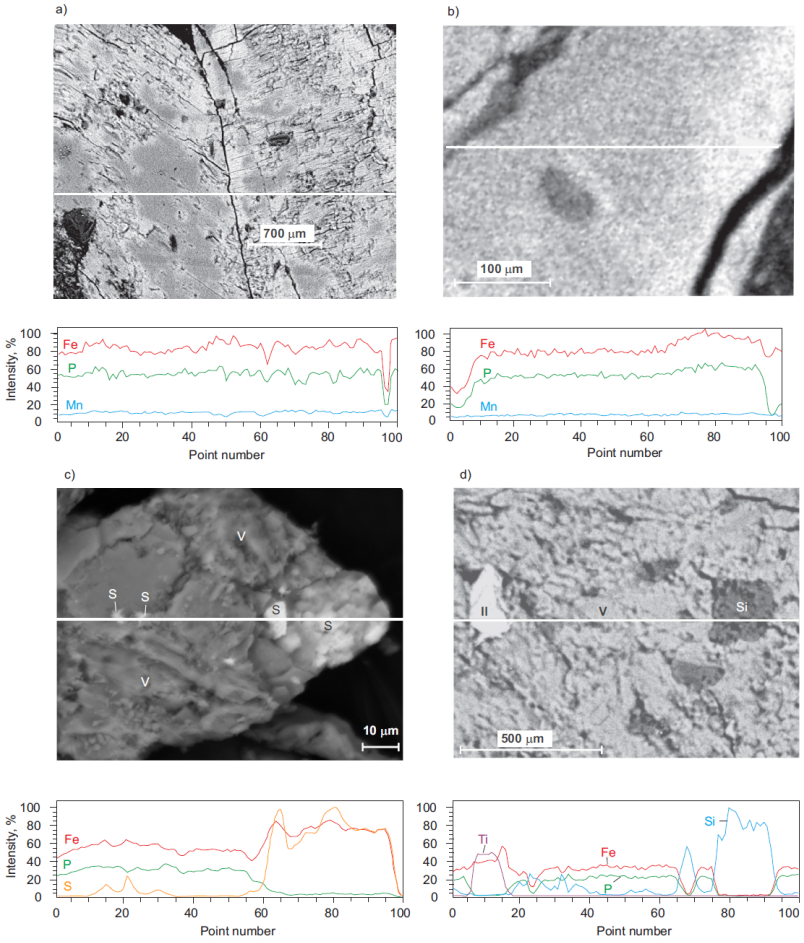

Fig. 4. Backscattered electron images of polished sections of vivianite nodules and energy dispersive spectroscopy. V – vivianite, S – sulfides, Il – ilmenite, Si – siliclastic.

CPD
8, 4989–5027, 2012

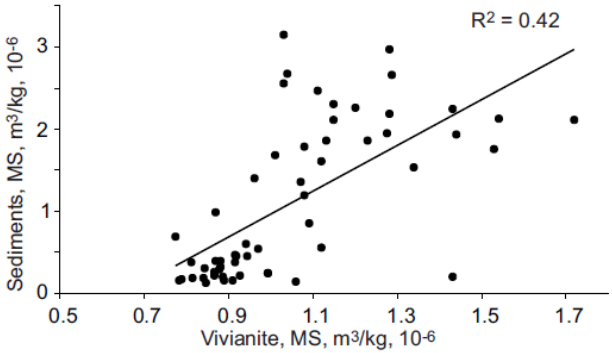

Fig. 5. Magnetic susceptibility of sediments versus magnetic susceptibility of vivianite nodules.

CPD
8, 4989–5027, 2012

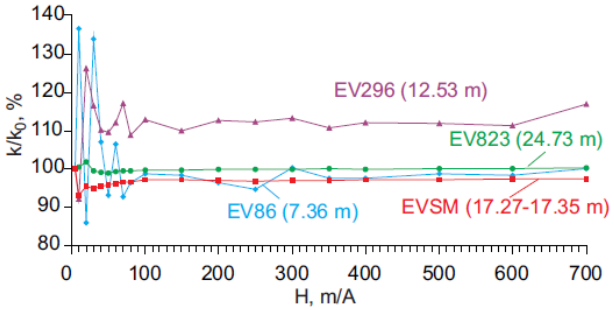

Fig. 6. The representative curves for four samples of susceptibility vs. field variation of vivianite.

CPD
8, 4989–5027, 2012

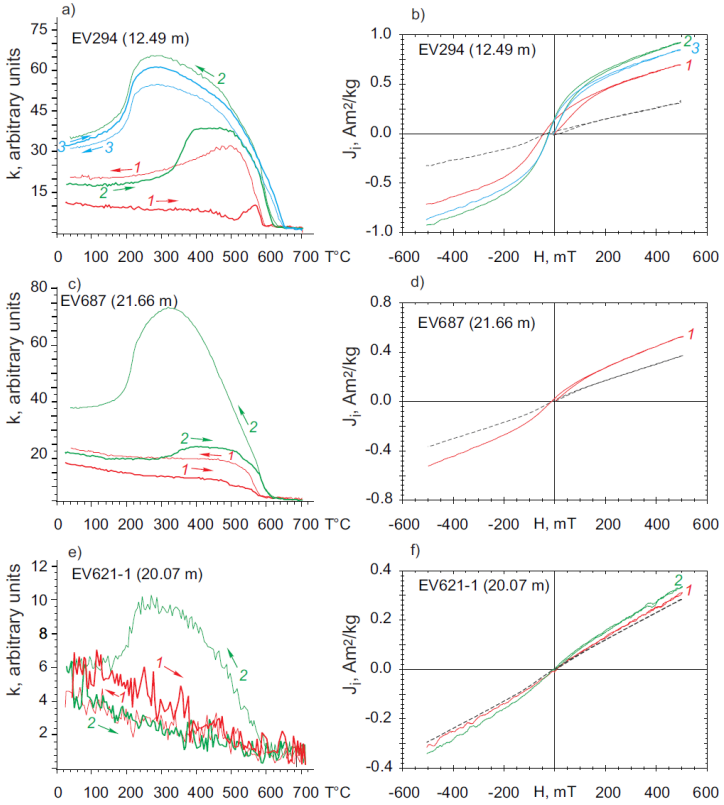

Fig. 7. Susceptibility versus temperature (in air) curves **(a, c, e)** of representative vivianite samples (the arrows indicate the heating and cooling curves, cursive number shows the heating and cooling runs) and typical examples of hysteresis loops (uncorrected for paramagnetism) of vivianite **(b, d, f)**.

CPD
8, 4989–5027, 2012

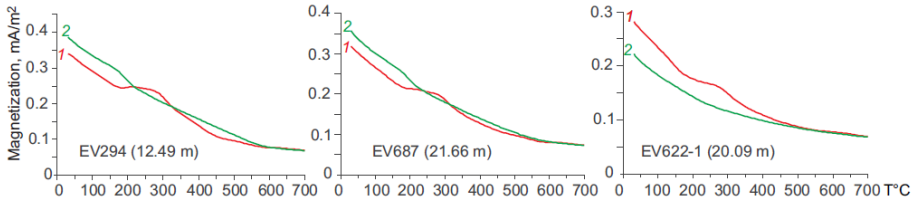

Fig. 8. Saturated magnetization versus temperature curves of representative vivianite samples. Cursive number shows the heating runs.

CPD
8, 4989–5027, 2012

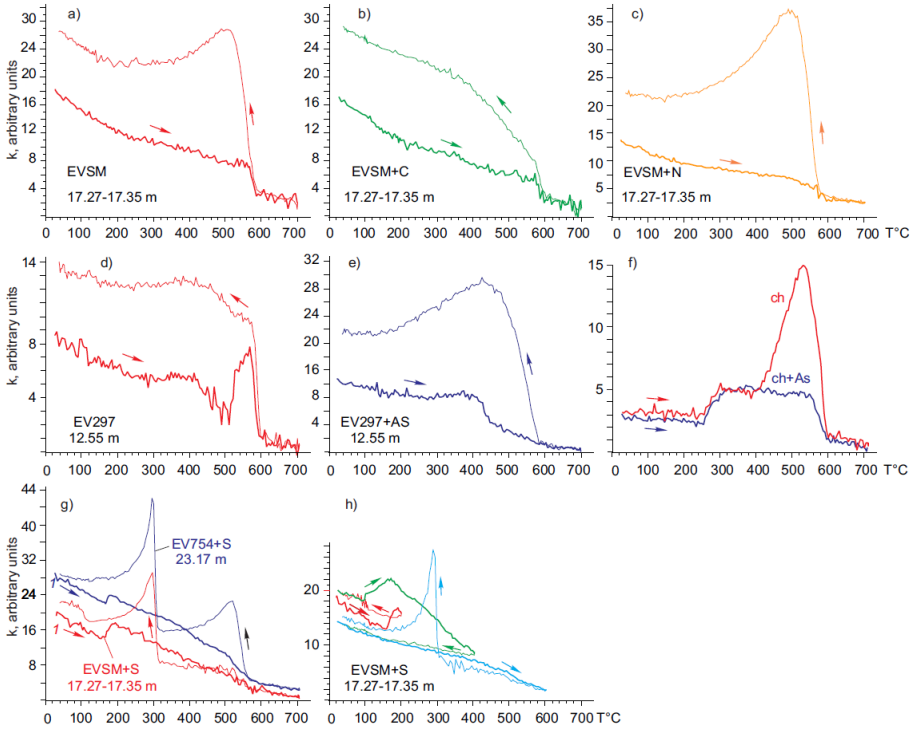

Fig. 9. Susceptibility versus temperature curves: **(a, d)** – in air; **(b)** – with sucrose; **(c)** – with carbamide; **(e)** – with arsenic; **(f)** chalcopyrite heating in air (ch) and with arsenic (ch + As); **(g, h)** with sulfur. The arrows indicate the heating and cooling runs.

CPD
8, 4989–5027, 2012

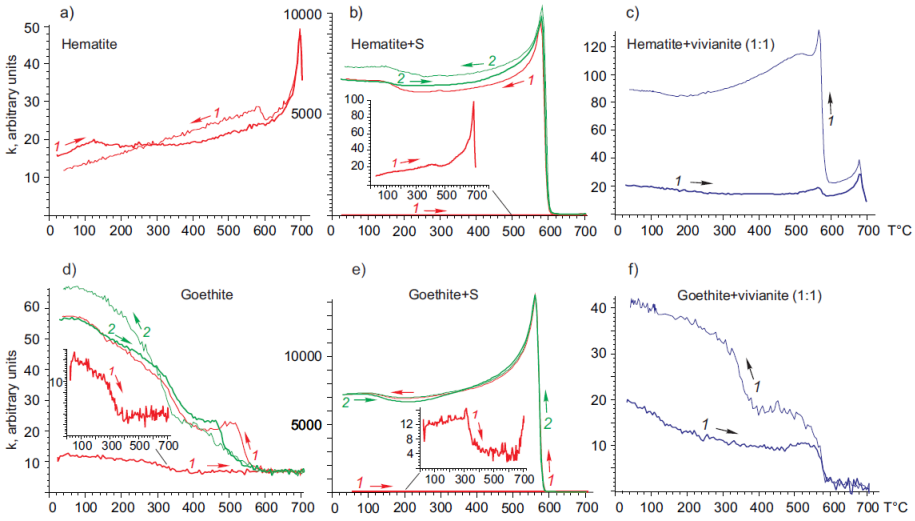

Fig. 10. Susceptibility versus temperature curves of hematite and goethite mixed with sulfur and with vivianite (1 : 1). The arrows and cursive numbers indicates the heating and cooling runs.

CPD
8, 4989–5027, 2012

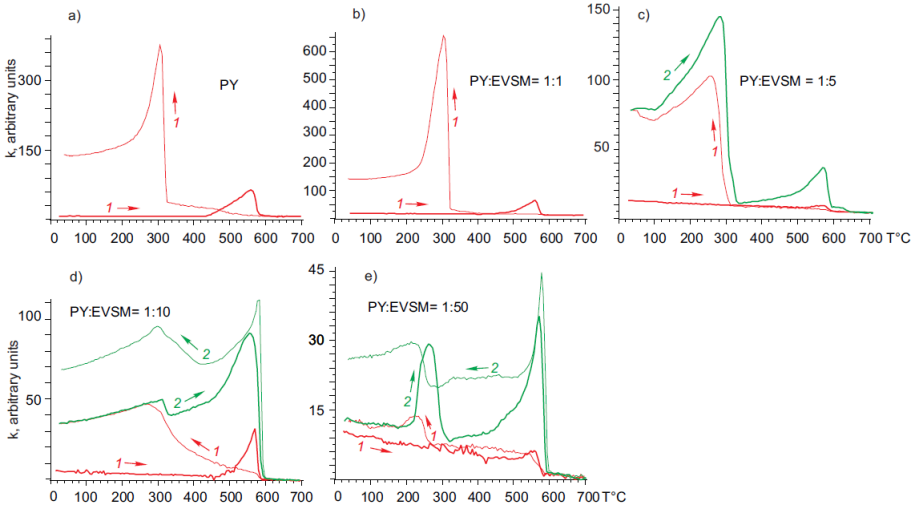

Fig. 11. Susceptibility versus temperature curves of pyrite and vivianite mixtures. The arrows and cursive numbers indicate the heating and cooling runs. PY – pyrite, EVSM – vivianite.

CPD
8, 4989–5027, 2012